

Optimized Kernel-based Projection Space of Riemannian Manifolds

Azadeh Alavi
University of Maryland

Vishal M Patel
Rutgers University

Rama Chellappa
University of Maryland

Abstract

Recent advances in computer vision suggest that encoding images through Symmetric Positive Definite (SPD) matrices can lead to increased classification performance. Taking into account manifold geometry is typically done via embedding the manifolds in tangent spaces, or Reproducing Kernel Hilbert Spaces (RKHS). Recently it was shown that projecting such manifolds into a kernel-based random projection space (RPS) leads to higher classification performance. In this paper, we propose to learn an optimized projection, based on building local and global sparse similarity graphs that encode the association of data points to the underlying subspace of each point. To this end, we project SPD matrices into an optimized distance preserving projection space (DPS), which can be followed by any Euclidean-based classification algorithm. Further, we adopt the concept of dictionary learning and sparse coding, and discriminative analysis, for the learned DPS on SPD manifolds. Experiments on face recognition, texture classification, person re-identification, and virus classification demonstrate that the proposed methods outperform state-of-the-art methods on such manifolds.

and similarity transforms. Despite its properties, methods using this approach have to deal with computational challenges, as non-linear operators are involved. To address the issue discussed above, two lines of research have been proposed in the literature: (1) embedding manifolds into manifold tangent spaces [25, 28, 37, 12]; and (2) embedding via the reproducing kernel Hilbert space (RKHS) [33, 18, 3]. Approaches under the first category in effect map points on manifolds to Euclidean spaces, thereby enabling the use of existing Euclidean-based learning algorithms, but at the cost of disregarding some of the manifold structure. Approaches under the second category address this by first mapping points on the manifold into RKHS, which can be considered as a high dimensional Euclidean space. Training data can be used to define a space that preserves manifold geometry [18]. The downside is that existing Euclidean-based learning algorithms need to be kernelised, which may not be trivial. Furthermore, the resulting methods can still have high computational load, making them impractical in more complex scenarios.

To address the discussed above drawbacks, the random projection method over RKHS (ROSE) [3], which combines the main advantage of tangent space approaches with the high accuracy provided by kernel space methods was recently proposed. By adapting a recent idea from techniques specifically designed for learning tasks in very large image datasets [15, 22], image representations are mapped into a reduced space wherein the similarities are still well-preserved [22]. The additional advantage of using such a method is that, the computational burden is considerably decreased while maintaining good classification performance. In other words, the proposed approach employs a mapping technique to create a space that preserves manifold geometry well, and can be considered as Euclidean.

However, the methods outlined above have some disadvantages. First, the dimensionality of the mapping matrix is unknown, and one can only rely on the historical data to compute appropriate dimensionality for each given application. In scenarios where the number of data is limited, deciding on proper dimensionality might not be feasible. In addition, as the name indicates, “Random Projection” is based on random sampling of the data. Hence, in

1. Introduction

In recent years, covariance matrices have been successfully used as image and video descriptors [4, 3, 26, 37], as they are known to provide compact and informative feature descriptions [5, 10]. Non-singular covariance matrices are Symmetric Positive Definite (SPD), and form connected Riemannian manifolds [24]. As such, to learn appropriate classifiers, the Riemannian geometry needs to be considered [37]. Affine Invariant Riemannian Metric (AIRM) can be considered as one of the most widely used similarity measures for SPD matrices [26]. The AIRM induces the Riemannian structure which is invariant to inversion

cases where the data size is sufficiently large, finding optimum random projection would require a very large number of random selections. As such, finding an optimum random projection can become impractical.

Contributions. In this paper, we propose to

- Learn the structure of the projection map by taking advantage of the concept of self-expressiveness property from subspace-sparse representation theory [12]. Thus, we construct both local and global sparse similarity graphs, whose nodes are connected to each other iff they correspond to points from the same subspace. To this end, we embed the SPD matrices into RKHS via the Stein Divergence Kernel¹, [35, 4]. Then we invoke the subspace-sparse representation theorem, and combine it with the random projection method over RKHS (ROSE). As such, we learn an appropriate projection which maps the embedded points into DPS.
- This is followed by utilizing any existing Euclidean-based learning algorithms, such as SVM. This does not violate the underlying structure of the SPD manifolds, as the proposed DPS preserves the manifold geometry. In addition, this mapping mitigates the drawbacks of the random projection on SPD manifolds method. Experiments on several vision tasks (person re-identification, face recognition, texture recognition, and virus classification), show that the proposed approach outperforms the random projection method over RKHS (ROSE) and several other state-of-the-art methods.
- Next, we adopt discriminative analysis (DA), and dictionary learning (DL) on the learned DPS of SPD manifolds. We further enhance the discriminative power of the method and extend the comparison of DPS-based with RKHS-based methods on SPD manifolds. Finally, we compare the performance of the proposed methods with other DA, and DL methods [18, 32, 16] on such manifolds.

Rest of the paper is organized as follows: Section 2 provides a brief overview of the manifold structure and its associated kernel function. Details of the Random Projection on RKHS of SPD manifolds are provided in Section 3. We then present the proposed approach in Section 4. Experimental results are provided in Section 5, and Section 6 concludes the paper with a brief summary and discussion.

¹We note, there are other SPD kernels that could be employed, such as Gaussian kernel [6, 19], or Stein based kernel on infinite-dimensional Covariance Descriptors [17]. However to keep the results comparable with previous works we use Stein Divergence Kernel in this paper.

2. Manifold structure and Stein Divergence Kernel

In this section, we first brief the SPD manifold geometry, and then introduce one of the SPD manifold kernels known as Stein Divergence [35].

Consider $\mathbb{X} = \{\mathbf{X}_1 \dots \mathbf{X}_n\} \in \mathcal{S}_d^+$ as a set of non-singular d by d covariance matrices, which are naturally SPD matrices. These matrices belong to smooth differentiable topological space, known as SPD manifolds. In this work, we endow the SPD manifold with the AIRM over its tangent spaces to induce the Riemannian structure into it [36]. We define the logarithm operation which maps points over the manifold to a tangent space as:

$$\log_{\mathbf{X}_i} \mathbf{X}_j = \mathbf{X}_i^{\frac{1}{2}} \log(\mathbf{X}_i^{-\frac{1}{2}} \mathbf{X}_j \mathbf{X}_i^{-\frac{1}{2}}) \mathbf{X}_i^{\frac{1}{2}}, \quad (1)$$

where $\mathbf{X}_i, \mathbf{X}_j \in \mathcal{S}_d^+$, \mathbf{X}_i is the point where the tangent space is located and \mathbf{X}_j is the point that we would like to map into the tangent space $\mathcal{T}_{\mathbf{X}_i} \mathcal{M}$; $\log(\cdot)$ is the matrix logarithm. The inverse function of this maps from points over a particular tangent space into the manifold defined via

$$\exp_{\mathbf{X}_i} \mathbf{y} = \mathbf{X}_i^{\frac{1}{2}} \exp(\mathbf{X}_i^{-\frac{1}{2}} \mathbf{y} \mathbf{X}_i^{-\frac{1}{2}}) \mathbf{X}_i^{\frac{1}{2}}, \quad (2)$$

where $\mathbf{X}_i \in \mathcal{S}_d^+$ is the tangent pole; $\mathbf{y} \in \mathcal{T}_{\mathbf{X}_i} \mathcal{M}$ is a point in the tangent space $\mathcal{T}_{\mathbf{X}_i} \mathcal{M}$; $\exp(\cdot)$ is the matrix exponential. Using these definitions, we now define the shortest distance between two points over the manifold. The geodesic distance [26], which is defined as the minimum length of the curvature path that connects between two points, can be written as:

$$d_g^2(\mathbf{X}_i, \mathbf{X}_j) = \text{trace}(\log^2(\mathbf{X}_i^{-\frac{1}{2}} \mathbf{X}_j \mathbf{X}_i^{-\frac{1}{2}})).$$

2.1. Stein Divergence Kernel

In this work, we employ the recently introduced Stein divergence [35] to calculate the distance between points on Riemannian manifolds. Stein divergence has an advantage of computational speed compare to geodesic distance, and is defined as follows

$$J_\phi(\mathbf{X}, \mathbf{Y}) \triangleq \log \left(\det \left(\frac{\mathbf{X} + \mathbf{Y}}{2} \right) \right) - \frac{1}{2} \log(\det(\mathbf{X}\mathbf{Y})). \quad (3)$$

Stein Divergence kernel is then defined based on the symmetric Stein divergence dissimilarity function

$$\mathbf{K}(\mathbf{X}, \mathbf{Y}) = e^{-\sigma J_\phi(\mathbf{X}, \mathbf{Y})}, \quad (4)$$

where $\mathbf{X}, \mathbf{Y} \in \mathcal{S}_{++}^d$ [35]. Consider $\{\mathbf{X}_1 \dots \mathbf{X}_n\}$ to be a set of matrices on the SPD manifold, the $n \times n$ matrix $\mathbb{K}_\sigma(i, j) = \mathbf{K}(\mathbf{X}_i, \mathbf{X}_j)$ defined in (4) is positive definite if the following condition is satisfied [34]

$$\sigma \in \left\{ \frac{1}{2}, \frac{2}{2}, \dots, \frac{n-1}{2} \right\}. \quad (5)$$

Therefore, if (5) is satisfied, (4) forms a Riemannian Kernel.

3. Random Projection over RKHS

The recently proposed approach known as ROSE, addresses image classification tasks originally formulated on the manifold by embedding them into a random projection space (Euclidean Space), while still respecting the underlying manifold structure. Random projection is an approximation method for estimating the dissimilarity between pairs of points in a high-dimensional space [1]. Basically, the projection of a point $\mathbf{u} \in \mathbb{R}^d$ can be done via a set of randomly generated hyperplanes $\{\mathbf{r}_1 \dots \mathbf{r}_k\} \in \mathbb{R}^d$

$$f(\mathbf{u}) = \mathbf{u}^\top \mathbf{W}, \quad (6)$$

where $\mathbf{W} \in \mathbb{R}^{d \times k}$ is the matrix wherein each column contains a single hyperplane \mathbf{r}_i ; $f(\cdot)$ is the mapping function which maps any point in \mathbb{R}^d into a reduced space \mathbb{R}^k . According to the Johnson-Lindenstrauss lemma [1], this mapping approximately preserves the pairwise distance between two points in the projected space.

Despite the popularity of the Johnson-Lindenstrauss lemma, many proposed methods restrict the distance function to l_p norm, the Mahalanobis metric, or the inner product [9, 11, 20], which makes them non-adaptable for non-Euclidean spaces. Recently, Kulis and Grauman [20] proposed a method that allows the distance function to be evaluated over RKHS. Thus, it is possible to apply the lemma for any arbitrary kernel $\mathbb{K}(i, j) = K(\mathbf{X}_i, \mathbf{X}_j) = \phi(\mathbf{X}_i)^\top \phi(\mathbf{X}_j)$ for an unknown embedding $\phi(\cdot)$ which maps the points to a Hilbert space \mathcal{H} [20]. This approach makes it possible for one to construct a random projection space over an SPD manifold, where the manifold structure is well-preserved.

As such, ROSE proposed to first map all the points over the manifold into RKHS via the Stein Divergence SPD kernel function $\phi(\cdot)$, and then map all the points in the RKHS $\phi(\mathbf{X}_i) \in \mathcal{H}$ into a random projection space \mathbb{R}^k with the aid of the recently introduced Kernelized Sensitive Hashing approach [20]. To achieve this, they follow Kulis-Grauman method [20] by randomly generating a set of hyperplanes over the RKHS $\{\mathbf{r}_1 \dots \mathbf{r}_k\} \in \mathcal{H}$ which are normalized to be approximately Gaussian. As the embedding function $\phi(\cdot)$ is considered as unknown, then the generation process is done indirectly via a weighted sum of the subset of the given training sets.

To this end, consider each data point $\phi(\mathbf{X}_i)$ from the training set as a vector from some underlying distribution D with unknown mean $\boldsymbol{\mu}$ and unknown covariance Σ . Let S be a set of t IID training exemplars from D , then $\mathbf{z}_t = \frac{1}{t} \sum_{i \in S} \phi(\mathbf{X}_i)$ is defined over S . According to the central limit theorem for sufficiently large t , the random vector $\mathbf{z}_t = \sqrt{t}(\mathbf{z}_t - \boldsymbol{\mu})$ is distributed as a multi-variate Gaussian $\mathcal{N}(\boldsymbol{\mu}, \Sigma)$ [30]. Then if the whitening transform: $\mathbf{r}_i = \Sigma^{-\frac{1}{2}} \mathbf{z}_i$ is applied which yields $\mathcal{N}(0, \Sigma)$ distribution in the Hilbert space \mathcal{H} . Therefore the i -th value of each vector in the

random projection space is defined as

$$\phi(\mathbf{X}_i)^\top \Sigma^{-\frac{1}{2}} \mathbf{z}_i. \quad (7)$$

As mean $\boldsymbol{\mu}$ and covariance Σ are unknown, they need to be estimated from the sample data. So a set of p objects from the dataset is chosen to form the first p items of the database: $\phi(\mathbf{X}_1) \dots \phi(\mathbf{X}_p)$. Then the mean is estimated as $\boldsymbol{\mu} = \frac{1}{p} \sum_{i=1}^p \phi(\mathbf{X}_i)$, and the covariance matrix Σ is also estimated using the p centred samples. Equation (7) can be computed using the Kernel PCA [20].

To summarize, the columns of the mapping matrix \mathbf{W} from (6), are calculated using

$$\mathbf{w}_i = \mathbf{K}^{\frac{1}{2}} \left(\frac{1}{t} \mathbf{e}_s - \frac{1}{p} \mathbf{1} \right), \quad (8)$$

where \mathbf{K} is the kernel matrix of Training data, $\mathbf{1}$ is a vector of all ones, and \mathbf{e}_s is a sparse vector with ones in the entries corresponding to the randomly selected positions [20].

4. Distance Preserving Projection Space for SPD Manifolds

In this section, we first introduce the proposed algorithm for learning the optimum Distance Preserving Projection on SPD manifolds (DPS). Then, we detail the steps for performing Graph Embedding Discriminative Analysis and Dictionary Learning over the proposed DPS of SPD manifolds.

The key idea for learning the optimized DPS is inspired by the 'self-expressiveness property of the data' from subspace sparse clustering method [12]. To be specific, we propose to model $\mathbf{K}^{\frac{1}{2}}$ structure through appropriately learned symmetric sparse similarity graphs. First, let us re-write (8) as follows:

$$\mathbf{W} = \alpha \mathbf{K}^{\frac{1}{2}} \mathbf{E} \quad (9)$$

, where $\alpha = \frac{(p-t)}{t}$, and $\mathbf{E} \in \mathbb{R}^{n \times t}$ is a $\{0, 1\}$ -matrix. It is widely acknowledged that even in cases where the number of collected samples is significantly smaller than the dimensionality of the data, the data set that needs to be processed usually exhibit significant structure, which often can be captured using sparsity models [7]. More specifically, it is shown that among the large sum possible representations of a given data point, in terms of other points, a sparse representation corresponds to selecting a few points from the same subspace [12].

As such, we learn the representing sparse codes for $\mathbf{K}^{\frac{1}{2}}$ by formulating a local self-expressive dictionary as follows:

$$\min(\|\mathbf{l}_i\|_1) \text{ s.t. } \bar{\mathbf{k}}_i = \mathbf{K}^{\frac{1}{2}} \mathbf{l}_i, \mathbf{L}_{ii} = 0. \quad (10)$$

, where $\mathbf{K}^{\frac{1}{2}} = [\bar{\mathbf{k}}_1 \bar{\mathbf{k}}_2 \dots \bar{\mathbf{k}}_n]$, and $\mathbf{L} = \{\mathbf{l}_1, \mathbf{l}_2, \dots, \mathbf{l}_n\}$ represents sparse codes. Although the sparse solution to (10)

captures valuable information about the relation between points, it is known to have limitations when it comes to dealing with points near the intersection of two subspaces [12]. To further enhance the method and resolve these limitations, we also encode the similarities between data points using the sparse solution of the global self-expressive dictionary, as follows:

$$\min(\|\mathbf{G}\|_1) \text{ s.t } \mathbf{K}^{\frac{1}{2}} = \mathbf{K}^{\frac{1}{2}}\mathbf{G}, \text{Diag}(\mathbf{G}_{ii}) = 0. \quad (11)$$

, where the sparse solutions to (10) and (11) can be efficiently computed by employing convex programming tools [8].

While the sparse solutions $\mathbf{L} = [\mathbf{l}_1 \ \mathbf{l}_2 \ \dots \ \mathbf{l}_n]$ and $\mathbf{G} = [\mathbf{g}_1 \ \mathbf{g}_2 \ \dots \ \mathbf{g}_n]$, ideally correspond to subspace sparse representations of the data points, they are not necessarily symmetric. However, it is clear that if $\bar{\mathbf{k}}_i$ and $\bar{\mathbf{k}}_j$ are members of the same subspace, i.e. $|\mathbf{L}_{ij}| > 0$ (or $|\mathbf{G}_{ij}| > 0$), then $\bar{\mathbf{k}}_j$ and $\bar{\mathbf{k}}_i$ must also be members of the same subspace, i.e respectively $|\mathbf{L}_{ji}| > 0$ (or $|\mathbf{G}_{ji}| > 0$). As such, we model local and global sparse symmetric similarity graphs $L = (\mathbf{V}^l, \mathbf{E}^l, \mathbf{W}^l)$ and $G = (\mathbf{V}^g, \mathbf{E}^g, \mathbf{W}^g)$, whose nodes resemble data points; where there is no edge between nodes that corresponds to points in different subspaces.

As such, we define the symmetric sparse similarity graphs as follows:

$$\mathbf{W}^l_{(i,j)} = \begin{cases} 1, & \text{if } \mathbf{E}^l_{ij} > 0 \text{ or } \mathbf{E}^l_{ji} > 0 \\ 0, & \text{otherwise} \end{cases} \quad (12)$$

$$\mathbf{W}^g_{(i,j)} = \begin{cases} 1, & \text{if } \mathbf{E}^g_{ij} > 0 \text{ or } \mathbf{E}^g_{ji} > 0 \\ 0, & \text{otherwise} \end{cases} \quad (13)$$

Considering (10) and (11), we reformulate (12) and (13) as follows:

$$\mathbf{W}^l_{(i,j)} = \begin{cases} 1, & \text{if } |\mathbf{L}_{ij}| > 0 \text{ or } |\mathbf{L}_{ji}| > 0 \\ 0, & \text{otherwise} \end{cases} \quad (14)$$

$$\mathbf{W}^g_{(i,j)} = \begin{cases} 1, & \text{if } |\mathbf{G}_{ij}| > 0 \text{ or } |\mathbf{G}_{ji}| > 0 \\ 0, & \text{otherwise} \end{cases} \quad (15)$$

Finally, Finally, to lean optimum distance preserving projection, we merge 9, 14, and 15 ²:

$$\mathbf{W} = \mathbf{K}^{\frac{1}{2}}([\alpha\mathbf{W}^l \quad \beta\mathbf{W}^g]) \quad (17)$$

To this end, we project each SPD matrix \mathbf{X}_i into distance preserving space (H-DPS) through bellow formulation:

$$\hat{\mathbf{k}}_i = \mathbf{k}(\mathbf{X}_i, \mathbb{X})\mathbf{K}^{\frac{1}{2}}([\alpha\mathbf{W}^l \quad \beta\mathbf{W}^g]) \quad (18)$$

²We can also form a local-based projection by merging (9) and (14):

$$\mathbf{W}^l = \mathbf{K}^{\frac{1}{2}}(\alpha\mathbf{W}^l) \quad (16)$$

, or similarly, formulate a global-based projection by merging (9) and (15). In experiment section we show that including both local and global information leads to improved classification performance.

We refer interested readers to [4, 20] for more detail.

In experiment section, we show that classification on the learned projection space outperforms other state of the art methods.

4.1. Graph Embedding Discriminative Analysis

In this section, we detail the procedure graph embedding discriminant analysis on DPS of SPD manifolds. As such, we propose to employ a method similar to the one discussed in [32], where the difference lies on projecting the SPD matrices into DPS rather than embedding such matrices into RKHS. In the experiment section, we show that the proposed graph embedding discriminant analysis based on DPS outperforms similar methods over RKHS.

A graph (\mathbf{V}, \mathbf{E}) in this context refers to a collection of vertices or nodes \mathbf{V} , and a collection of edges that connect pairs of vertices. We note that \mathbf{E} is a symmetric matrix with elements describing the similarity between pairs of vertices. Moreover, the diagonal matrix \mathbf{D} and the Laplacian matrix \mathbf{L} of a graph are defined as $\mathbf{L} = \mathbf{D} - \mathbf{E}$, with the diagonal elements of \mathbf{D} obtained as $\mathbf{D}(i, i) = \sum_j \mathbf{E}(i, j)$.

Let φ be the function that projects SPD matrices into DPS. As such, using (18) :

$$\begin{aligned} \varphi(\mathbf{X}_i) &= \mathbf{k}(\mathbf{X}_i, \mathbb{X})\mathbf{K}^{\frac{1}{2}}([\alpha\mathbf{W}^l \quad \beta\mathbf{W}^g]) \\ &= \hat{\mathbf{k}}_i \end{aligned} \quad (19)$$

Given N labelled points $\mathbb{X} = \{(\mathbf{X}_i, l_i)\}_{i=1}^N$ from the underlying SPD manifold \mathcal{S}_d^+ , where $l_i \in \{1, 2, \dots, C\}$; and $\hat{\mathbb{K}} = \{(\hat{\mathbf{k}}_i, l_i)\}_{i=1}^N$ from the training set on the learned DPS; the local structure of the data can be modeled by building a within-class similarity graph \mathbf{E}_w and a between-class similarity graph \mathbf{E}_b . The simplest forms of \mathbf{E}_w and \mathbf{E}_b are based on the nearest neighbour graphs defined below:

$$\mathbf{E}_w(i, j) = \begin{cases} 1, & \text{if } \hat{\mathbf{k}}_i \in N_w(\hat{\mathbf{k}}_j) \text{ or } \hat{\mathbf{k}}_j \in N_w(\hat{\mathbf{k}}_i) \\ 0, & \text{otherwise} \end{cases} \quad (20)$$

$$\mathbf{E}_b(i, j) = \begin{cases} 1, & \text{if } \hat{\mathbf{k}}_i \in N_b(\hat{\mathbf{k}}_j) \text{ or } \hat{\mathbf{k}}_j \in N_b(\hat{\mathbf{k}}_i) \\ 0, & \text{otherwise} \end{cases} \quad (21)$$

In (20), $N_w(\hat{\mathbf{k}}_i)$ is the set of v_w neighbours $\{\hat{\mathbf{k}}_1^1, \hat{\mathbf{k}}_1^2, \dots, \hat{\mathbf{k}}_1^{v_w}\}$, sharing the same label as l_i . Similarly in (eqrefeqn:Gb), $N_b(\hat{\mathbf{k}}_i)$ contains v_b neighbours having different labels.

Our aim is to simultaneously maximize a measure of discriminatory power and preserve the geometry of points. This can be formalised by finding $\mathbb{W} : \varphi(\mathbf{X}_i) \rightarrow \mathbf{y}_i$ such that the connected points of \mathbf{E}_w are placed as close as possible, while the connected points of \mathbf{E}_b are moved as far as possible. The mapping is sought by optimising the following

two objective functions:

$$f_1 = \min \frac{1}{2} \sum_{i,j} \|\mathbf{y}_i - \mathbf{y}_j\|^2 \mathbf{E}_w(i,j) \quad (22)$$

$$f_2 = \max \frac{1}{2} \sum_{i,j} \|\mathbf{y}_i - \mathbf{y}_j\|^2 \mathbf{E}_b(i,j) \quad (23)$$

Eqn. (22) punishes neighbours in the same class if they are mapped far away, while Eqn. (23) punishes points of different classes if they are mapped close together. According to the representer theorem [31], the solution $\mathbb{W} = [\gamma_1 | \gamma_2 | \dots | \gamma_r]$, can be expressed as a linear combination of data points, *i.e.*, $\gamma_i = \sum_{j=1}^N w_{i,j} \varphi(\mathbf{X}_j)$:

$$\mathbf{Y}_i = (\langle \gamma_1, \varphi(\mathbf{X}_i) \rangle, \langle \gamma_2, \varphi(\mathbf{X}_i) \rangle, \dots, \langle \gamma_r, \varphi(\mathbf{X}_i) \rangle)^T \quad (24)$$

Since :

$$\begin{aligned} & \langle \gamma_l, \varphi(\mathbf{X}_i) \rangle \\ &= \sum_{j=1}^N w_{l,j} (\mathbf{k}(\mathbf{X}_i, \mathbf{X}_j) \mathbf{K}^{\frac{1}{2}} [(\alpha \mathbf{W}^l) \quad (\beta \mathbf{W}^g)])^T \\ &= \sum_{j=1}^N w_{l,j} \hat{\mathbf{k}}_j \end{aligned} \quad (25)$$

,then $\mathbf{Y}_i = \mathbf{W}^T \hat{\mathbf{k}}_i$, where:

$$\mathbf{W} = \begin{pmatrix} w_{1,1} & w_{1,2} & \dots & w_{1,r} \\ w_{2,1} & w_{2,2} & \dots & w_{2,r} \\ \vdots & \vdots & \vdots & \vdots \\ w_{N,1} & w_{N,2} & \dots & w_{N,r} \end{pmatrix}$$

Substitution of this into (22) results in:

$$\begin{aligned} & \frac{1}{2} \sum_{i,j} \|\mathbf{y}_i - \mathbf{y}_j\|^2 \mathbf{E}_w(i,j) \\ &= \frac{1}{2} \sum_{i,j} \|\mathbf{W}^T \hat{\mathbf{k}}_i - \mathbf{W}^T \hat{\mathbf{k}}_j\|^2 \mathbf{E}_w(i,j) \\ &= \text{Tr}(\mathbf{W}^T \hat{\mathbb{K}} \mathbf{D}_w \hat{\mathbb{K}}^T \mathbf{W}) - \text{Tr}(\mathbf{W}^T \hat{\mathbb{K}} \mathbf{E}_w \hat{\mathbb{K}}^T \mathbf{W}) \end{aligned} \quad (26)$$

where $\hat{\mathbb{K}} = [\hat{\mathbf{k}}_1 \hat{\mathbf{k}}_2 \dots \hat{\mathbf{k}}_N]$. Considering that $\mathbf{L}_b = \mathbf{D}_b - \mathbf{W}_b$, in a similar manner it can be shown that (23) can be simplified to:

$$\begin{aligned} & \frac{1}{2} \sum_{i,j} \|\mathbf{y}_i - \mathbf{y}_j\|^2 \mathbf{E}_b(i,j) \\ &= \text{Tr}(\mathbf{W}^T \hat{\mathbb{K}} \mathbf{D}_b \hat{\mathbb{K}}^T \mathbf{W}) - \text{Tr}(\mathbf{W}^T \hat{\mathbb{K}} \mathbf{E}_b \hat{\mathbb{K}}^T \mathbf{W}) \\ &= \text{Tr}(\mathbf{W}^T \hat{\mathbb{K}} \mathbf{L}_b \hat{\mathbb{K}}^T \mathbf{W}) \end{aligned} \quad (27)$$

As a result, the max versions of (22) and (23) can be merged by the Lagrangian method as follows:

$$\begin{aligned} & \max \{ \text{Tr}(\mathbf{W}^T \hat{\mathbb{K}} (\mathbf{L}_b + \beta \mathbf{E}_w) \hat{\mathbb{K}}^T \mathbf{W}) \} \\ & \text{subject to } \text{Tr}(\mathbf{W}^T \hat{\mathbb{K}} \mathbf{D}_w \hat{\mathbb{K}}^T \mathbf{W}) = 1 \end{aligned} \quad (28)$$

where β is a Lagrangian multiplier, and $\mathbf{L}_b = \mathbf{D}_b - \mathbf{W}_b$. The solution to the optimisation in (28) corresponds to the r largest eigenvectors of the following generalised eigenvalue problem [32]:

$$\hat{\mathbb{K}} \{ \mathbf{L}_b + \beta \mathbf{E}_w \} \hat{\mathbb{K}}^T \mathbf{W} = \lambda \hat{\mathbb{K}} \mathbf{D}_w \hat{\mathbb{K}}^T \mathbf{W} \quad (29)$$

The experiment result indicates that the propose DPS-based Graph Embedding outperforms the RKHS-based Graph Embedding Discriminant Analysis.

4.2. Dictionary Learning and Sparse Coding

In this section, we describe DPS-based dictionary learning and sparse coding on SPD manifolds. First, we project the SPD matrices into DPS through (18), which is followed by jointly minimizing the following energy function, *i.e.*, $\min(J_{\text{DVS}})$

$$J = \sum_{j=1}^n \left(\left\| \hat{\mathbf{k}}_j - \sum_{i=1}^n \mathbf{v}_{j,i} (\hat{\mathbf{D}}_i) \right\|^2 + \lambda \|\mathbf{v}_j\|_1 \right), \mathbf{v}_j \in \mathbb{R}^n \quad (30)$$

, where $\mathbf{X}_j \in \mathcal{S}_d^+$, and $\hat{\mathbf{k}}_j$ is a of the SPD matrix on DPS, $\mathbb{V} = \{\mathbf{v}_1, \mathbf{v}_2, \dots, \mathbf{v}_n\}$ represents the sparse codes, $\hat{\mathbf{D}} = \{\hat{\mathbf{D}}_1, \hat{\mathbf{D}}_2, \dots, \hat{\mathbf{D}}_n\}$ is a DPS-based dictionary. Then we employ KSVD[2] over the SPD, to solves the optimization iteratively. Experiments indicate that the proposed DPS-based Dictionary Learning and Sparse Coding outperforms state of the art dictionary learning algorithm on SPD manifolds.

5. Experiments and Discussion

In this section, we investigate the performance of the proposed Distance Preserved Projection on SPD manifolds (DPS) ³ [35, 4], through two sets of experiments. First, we evaluate the proposed DPS-based classification and compare the performance with an RKHS-based (S-SVM) [17], and Random-Projection-based (ROSE)⁴ [4] classification methods. We also examine the effect of including both local and global information in the proposed hybrid method. Thus, we refer to the hybrid-projection based DPS using (17), as (H-DPS). Similarly, we refer to the local-projection based DPS using (16), as (L-DPS), and the global-projection based DPS as (G-DPS).

Next, we study the performance of proposed Graph Embedding Discriminate Analysis on DPS (DPS-DA) with the RKHS-based Discriminative analysis (RGEDA) [32]. This is then followed by evaluating the proposed DPS-based dictionary learning and comparing the performance with RKHS-Based dictionary learning for SPD manifolds [18, 16].

We validate the proposed method using four datasets as follows: (1) Texture classification [27]; (2) Face recognition [26]; (3) Person re-identification [29]; and (4) Virus Texture Classification [21].

³We note, there are other SPD kernels that could be employed, such as Gaussian kernel [6, 19], or the Stein based kernel on infinite-dimensional Covariance Descriptors [17]. However to keep the results comparable with previous works we use Stein Divergence Kernel in this paper.

⁴We note that it has been shown that adding synthetic data would help to increase the classification performance in some cases ROSES[4]. However, for some applications, *i.e.* face recognition, it causes performance decrease [4]; as such, we choose not to add synthetic data in this work

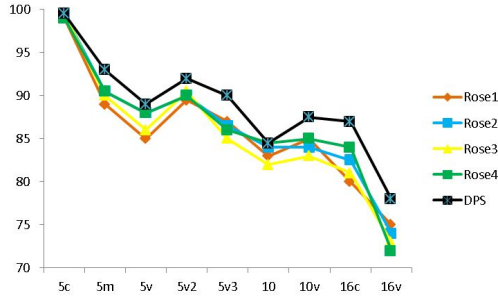


Figure 1: Comparing classification performance of random projection (5 runs) on the Brodatz texture dataset, with DPS on the same dataset.

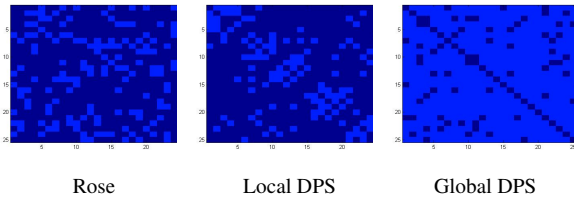


Figure 2: Examples of projection maps on sequence 5c of Brodatz dataset. From left to right : Projection map of Rose (E in 9), Projection map of Local DPS (W^l in 12), and Projection map of Global DPS (W^g in 13).

5.1. Classification

We start by examining the fluctuation in classification performance using ROSE. We repeat the experiment five times and show how the result varies in each run. Figure 1 illustrates the results for the texture recognition dataset (details on dataset can be found in Section 5.1.2), and shows that the proposed SPD-based classification method outperforms ROSE in all the cases. To provide more insight, Fig. 2 demonstrates examples of projection maps in ROSE and SPD.

5.1.1 Virus Classification

The virus dataset [21] contains 15 different virus classes, where each class has hundreds of 41×41 images that were segmented automatically [21]. Samples from the virus dataset are shown in Fig. 3. Following the same protocol as

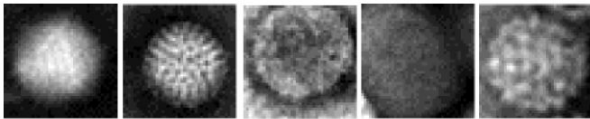


Figure 3: Examples of images from the virus dataset [21].

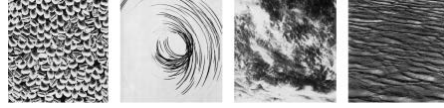


Figure 4: Samples of Brodatz texture dataset [27].

in [18, 16] we used the 10 splits provided within the dataset in a 10 fold cross validation manner, i.e., 10 experiments with 9 splits for training and 1 split as test.

At each pixel $p = (x, y)$ of an image, we then computed the 25-dimensional feature vector as following:

$$F_p = \left[I_p, \left| \frac{\partial I}{\partial x} \right|, \left| \frac{\partial I}{\partial y} \right|, \left| \frac{\partial^2 I}{\partial x^2} \right|, \left| \frac{\partial^2 I}{\partial y^2} \right|, |G_{0,0}(x, y)|, \dots, |G_{4,7}(x, y)| \right]$$

We report the mean recognition accuracies over the 10 runs. Table 1 shows that the proposed DPS outperforms S-SVM, ROSE, and the PLS-based Covariance Discriminant Learning (CDL) technique [38], which is considered as a state of the art technique. We also observed that the generating Hybrid method advances the performance of DSP (%78.7), and outperforms both global (%78), and local DPS(%77.6).

	CDL	S-SVM	ROSE	H-DPS
Average	69.5 ± 3.1	76.5 ± 3.3	76 ± 4.1	78.7 ± 3.2

Table 1: Recognition accuracy (in %) on the Virus classification dataset

5.1.2 Texture Classification

To examine the performance of the propose DPS on classification using the Brodatz texture dataset [27] (Examples are shown in Fig. 4, we follow the test protocol advised in [33].

Nine test scenarios with various number of classes were generated. The test scenarios included 5-texture ('5c', '5m', '5v', '5v2', '5v3'), 10-texture ('10', '10v') and 16-texture ('16c', '16v') mosaics. To create a Riemannian manifold, we follow the same protocol as described in [4, 32]. As such, we first downsample each image to 256×256 , followed by splitting them into 64 regions of size 32×32 . The feature vector for each pixel $I(x, y)$ is defined as:

$$F(x, y) = \left[I(x, y), \left| \frac{\partial I}{\partial x} \right|, \left| \frac{\partial I}{\partial y} \right|, \left| \frac{\partial^2 I}{\partial x^2} \right|, \left| \frac{\partial^2 I}{\partial y^2} \right| \right]$$

Table 2 shows that in all the sequences (DPS-based classification outperforms both S-SVM, and in all but one sequence (for which they perform on par), it outperforms ROSE. It also illustrates that on average, generating Hybrid method advances the performance of DSP, and outperforms both global (%88.5) and local DPS (%88.1).

	S-SVM	ROSE	H-DPS
5c	99.5	99.3	99.5
5m	86	90.1	93
5v	86.5	91.6	91.6
5v2	89.5	90.5	92
5v3	87.5	88.6	90
10	81.5	86.7	86.7
10v	81.5	88.1	88.1
16c	80	84.1	87
16v	73.5	77.1	78
Average	84.9	88.5	89.5

Table 2: Recognition accuracy (in %) for the BRODATZ texture recognition dataset. task on BRODATZ dataset

5.1.3 Face Recognition

For the face recognition task, we follow the same protocol as described in [4, 32]. We consider the subset 'b' of the FERET dataset [26]. This subset includes 1400 images from 198 subjects. Each image is closely cropped to merely include the face and then downsampled to 64×64 . Figure 5 shows examples of the FERET dataset.

To evaluate the performance, we created three tests with various pose angles. In all the tests, training data consisted of the images labeled as 'bj', 'bk' and 'bf' (ie., frontal image with illumination, expression and small pose variations). Images marked as 'bd', 'be' and 'bg' (ie., non-frontal images) were used as three separate test sets. In our method, each face image is represented by a 43×43 covariance matrix as a point on the Riemannian manifold. To this end, for every pixel $I(x, y)$, we then computed $G_{u,v}(x, y)$ as the response of a 2D Gabor wavelet ($G_{u,v}(x, y)$) [23], centered at x, y with orientation u and scale v . Then the feature vector is defined as following:

$$F_{x,y} = [I(x,y), x, y, |G_{0,0}(x,y)|, \dots, |G_{4,7}(x,y)|]$$

Table 3 illustrates the performance of DPS on FERET face recognition dataset, and shows that DPS outperforms both S-SVM and ROSE. In addition, it shows that in all the cases hybrid (%91.5) and global methods perform on par, and outperform the local (%91) DPS.



Figure 5: Examples of closely-cropped faces from the FERET 'b' subset.

	S-SVM	ROSE	H-DPS
bg	69.5	80	85
bf	95	95	98
be	82	85	94
bd	52	70.5	75.5
Average	74.6	82.6	91.5

Table 3: Recognition accuracy (in %) for the face recognition task on the b subset of the FERET dataset



Figure 6: Examples of pedestrians in the ETHZ dataset.

5.1.4 Person Re-identification

In this section we test the performance of the proposed DPS method for person reidentification task on the modified ETHZ dataset [29], and follow the same protocol described in [4, 32]. The original version of this dataset was captured from a moving camera [13], and it has been used for human detection. The main challenging aspects of ETHZ dataset are variations in pedestrians appearances and occlusions. Some sample images of the ETHZ dataset are shown in figure 6. This dataset contains three video sequences. We downsampled all the images to 64×32 . For each subject, the training set consists of 10 randomly selected images and the rest used for the test set. To generalise the practical assessment of the algorithm, random selection of the training and testing data was repeated 20 times.

To create points on the Riemannian manifold, a feature vector was formed for each pixel using the position of the pixel (x and y), the corresponding colour information ($R_{x,y}$, $G_{x,y}$ and $B_{x,y}$) and the gradient and Laplacian for colour C , defined as $C'_{x,y} = [|\partial C / \partial x|, |\partial C / \partial y|]$ and $C''_{x,y} = [|\partial^2 C / \partial x^2|, |\partial^2 C / \partial y^2|]$, respectively. Then the representation for each image is the covariance matrix using the following feature:

$$F_{x,y} = [x, y, R_{x,y}, G_{x,y}, B_{x,y}, R'_{x,y}, G'_{x,y}, B'_{x,y}, R''_{x,y}, G''_{x,y}, B''_{x,y}]$$

	S-SVM	ROSE	H-DPS
Seq.1	84.4 ± 1	90.7 ± 0.9	90.7 ± 0.9
Seq.2	84.2 ± 1.3	91.5 ± 1.7	92.7 ± 1.5
Average	84.3	91.2	91.7

Table 4: Recognition accuracy (in %) for the person re-identification task on Seq.1 and Seq.2 of the ETHZ dataset

Table 4 shows that on average, DPS outperforms both S-SVM and ROSE. We also observed that the hybrid DPS (%91.7) advances the method and outperforms both local (%91.5) and global DPS (%91).

5.1.5 Further Analysis

To further examine the performance of the proposed DPS, we compare the proposed DPS-based graph embedding discriminant analysis (DPS-DA) with the similar RKHS-based method (RGEDA)[32]. In addition we compare the proposed DPS-based dictionary learning and sparse coding (DPS-DI) method with kernel-based dictionary learning and sparse coding on SPD manifold (RSR) [18]. [16]. Table.

	TSC	RGEDA	DPS-DA	RSR	DPS-DI
5c	100	99	100	99.5	99.5
5m	75	83	91.5	84	91.5
5v	82.5	83	91.5	89	89
5v2	82	85	92	89.5	91.5
5v3	81.5	82	90	86	89
10	81	83	85	83	83
10v	68	81	89	86.5	87
16c	77	82	87.5	82	84
16v	66	77.5	78.5	77	79
Average	79.4	84	89.5	86.3	88.2

Table 5: Recognition accuracy (in %) for the BRODATZ texture recognition dataset.

5 shows that on average DPS-based discriminative analysis outperforms RKHS-based discriminative analysis in all the sequences of the BRODATZ dataset. It performs on par with TSC, which is considered as state of the art method, on 5c sequence, and outperforms TSC on all the other sequences. On average DPS-based dictionary learning and sparse coding outperforms both TSC and RSR. Table. 6

	SDALF	RGEDA	DPS-DA	RSR	DPS-DI
Seq.1	83.4	90.5	92	91	92
Seq.2	83.4	92	93.5	92	92.5
Average	83.4	91.3	92.7	91.5	92.2

Table 6: Recognition accuracy (in %) for the person re-identification task on Seq.1 and Seq.2 of the ETHZ dataset

shows that on average DPS-based discriminative analysis outperforms RGDA, RKHS-based discriminative analysis, on ETHZ dataset. It also outperforms SDALF in all the cases DPS outperforms SDALF [14], which is considered to be the state of the art. It also illustrates that DPS-based dictionary learning and sparse coding outperforms RSR and

	CDL	RGEDA	DPS-DA	RSR	DPS-DI
Average	69.5	77.9	78.7	78	79

Table 7: Recognition accuracy (in %) for the Virus Texture Recognition dataset

SDALF in all the cases. Table. 7 shows that on average the DPS-based discriminative analysis outperforms RGEDA, CDL [38] which is considered as state of the art, on the Virus Texture dataset. It also illustrates that DPS-based dictionary learning and sparse coding outperforms both RSR and CDL.

6. Conclusion

In this paper, we propose to learn the optimum kernel-based projection that maps SPD matrices into a Distance Preserving Projection Space (DPS), through constructing both local and global sparse similarity graphs, whose nodes are connected to each other iff they correspond to points from the same subspace. We show that a such mapping mitigates the drawbacks of the random projection on SPD manifolds method. Experiments on several vision tasks (person re-identification, face recognition, texture recognition, and virus classification), show that the proposed approach outperforms ROSE and several other state-of-the-art methods. We further adopt discriminative analysis (DA), and dictionary learning (DL) on the learned DPS of such manifolds, and show that such methods outperform state of the art methods on SPD manifolds.

References

- [1] D. Achlioptas. Database-friendly random projections: Johnson-lindenstrauss with binary coins. *Journal of computer and System Sciences*, 66(4):671–687, 2003. 3
- [2] M. Aharon, M. Elad, and A. Bruckstein. An algorithm for designing overcomplete dictionaries for sparse representation. *Signal Processing, IEEE Transactions on*, 54(11):4311–4322, 2006. 5
- [3] A. Alavi, M. T. Harandi, and C. Sanderson. Relational divergence based classification on riemannian manifolds. In *Applications of Computer Vision (WACV), 2013 IEEE Workshop on*, pages 111–116. IEEE, 2013. 1
- [4] A. Alavi, A. Wiliem, K. Zhao, B. C. Lovell, and C. Sanderson. Random projections on manifolds of symmetric positive definite matrices for image classification. In *Applications of Computer Vision (WACV), 2014 IEEE Winter Conference on*, pages 301–308. IEEE, 2014. 1, 2, 4, 5, 6, 7
- [5] C. Anoop, M. Vassilios, and P. Nikolaos. Dirichlet process mixture models on symmetric positive definite matrices for appearance clustering in video surveillance applications. In *IEEE Conf. Computer Vision and Pattern Recognition (CVPR)*, pages 3417–3424, 2011. 1

- [6] V. Arsigny, P. Fillard, X. Pennec, and N. Ayache. Log-euclidean metrics for fast and simple calculus on diffusion tensors. *Magnetic resonance in medicine*, 56(2):411–421, 2006. 2, 5
- [7] S. Bahmani, B. Raj, and P. T. Boufounos. Greedy sparsity-constrained optimization. *The Journal of Machine Learning Research*, 14(1):807–841, 2013. 3
- [8] S. Boyd and L. Vandenberghe. *Convex optimization*. Cambridge university press, 2004. 4
- [9] M. S. Charikar. Similarity estimation techniques from rounding algorithms. In *Proceedings of the thirty-fourth annual ACM symposium on Theory of computing*, pages 380–388. ACM, 2002. 3
- [10] A. Cherian, S. Sra, A. Banerjee, and N. Papanikolopoulos. Efficient similarity search for covariance matrices via the Jensen-Bregman LogDet divergence. In *Int. Conf. Computer Vision (ICCV)*, pages 2399–2406, 2012. 1
- [11] M. Datar, N. Immorlica, P. Indyk, and V. S. Mirrokni. Locality-sensitive hashing scheme based on p-stable distributions. In *Proceedings of the twentieth annual symposium on Computational geometry*, pages 253–262. ACM, 2004. 3
- [12] E. Elhamifar and R. Vidal. Sparse subspace clustering: Algorithm, theory, and applications. *Pattern Analysis and Machine Intelligence, IEEE Transactions on*, 35(11):2765–2781, 2013. 1, 2, 3, 4
- [13] A. Ess, B. Leibe, and L. Van Gool. Depth and appearance for mobile scene analysis. In *Int. Conf. Computer Vision (ICCV)*, pages 1–8, 2007. 7
- [14] M. Farenzena, L. Bazzani, A. Perina, V. Murino, and M. Cristani. Person re-identification by symmetry-driven accumulation of local features. *IEEE Conf. Computer Vision and Pattern Recognition*, pages 2360–2367, 2010. 8
- [15] K. Guo, P. Ishwar, and J. Konrad. Action recognition using sparse representation on covariance manifolds of optical flow. In *Advanced Video and Signal Based Surveillance (AVSS), 2010 Seventh IEEE International Conference on*, pages 188–195. IEEE, 2010. 1
- [16] M. Harandi and M. Salzmann. Riemannian coding and dictionary learning: Kernels to the rescue. 2015. 2, 5, 6, 8
- [17] M. Harandi, M. Salzmann, and F. Porikli. Bregman divergences for infinite dimensional covariance matrices. In *Computer Vision and Pattern Recognition (CVPR), 2014 IEEE Conference on*, pages 1003–1010. IEEE, 2014. 2, 5
- [18] M. T. Harandi, C. Sanderson, R. Hartley, and B. C. Lovell. Sparse coding and dictionary learning for symmetric positive definite matrices: A kernel approach. In *Computer Vision—ECCV 2012*, pages 216–229. Springer, 2012. 1, 2, 5, 6, 8
- [19] S. Jayasumana, R. Hartley, M. Salzmann, H. Li, and M. Harandi. Kernel methods on riemannian manifolds with gaussian rbf kernels. 2015. 2, 5
- [20] B. Kulis and K. Grauman. Kernelized locality-sensitive hashing. *Pattern Analysis and Machine Intelligence, IEEE Transactions on*, 34(6):1092–1104, 2012. 3, 4
- [21] G. Kylberg, M. Uppström, K.-O. HEDLUND, G. Borgefors, and I.-M. SINTORN. Segmentation of virus particle candidates in transmission electron microscopy images. *Journal of microscopy*, 245(2):140–147, 2012. 5, 6
- [22] S. Lang. *Fundamentals of differential geometry*, volume 160. Springer Verlag, 1999. 1
- [23] T. Lee. Image representation using 2d Gabor wavelets. *IEEE Transactions on Pattern Analysis and Machine Intelligence*, 18(10):959–971, 1996. 7
- [24] Y. Lui. Tangent bundles on special manifolds for action recognition. *IEEE Trans. Circuits and Systems for Video Technology*, 22(6):930–942, 2011. 1
- [25] X. Pennec. Intrinsic statistics on Riemannian manifolds: Basic tools for geometric measurements. *Journal of Mathematical Imaging and Vision*, 25(1):127–154, 2006. 1
- [26] P. Phillips, H. Moon, S. Rizvi, and P. Rauss. The FERET evaluation methodology for face-recognition algorithms. *IEEE Trans. Pattern Analysis and Machine Intelligence*, 22(10):1090–1104, 2000. 1, 2, 5, 7
- [27] T. Randen and J. Husoy. Filtering for texture classification: A comparative study. *IEEE Transactions on Pattern Analysis and Machine Intelligence*, 21(4):291–310, 1999. 5, 6
- [28] T. Randen and J. H. Husøy. Filtering for texture classification: A comparative study. *IEEE Trans. Pattern Analysis and Machine Intelligence*, 21(4):291–310, 1999. 1
- [29] W. Schwartz and L. Davis. Learning discriminative appearance-based models using partial least squares. In *Brazilian Symposium on Computer Graphics and Image Processing (SIBGRAPI)*, pages 322–329. IEEE, 2009. 5, 7
- [30] W. R. Schwartz and L. S. Davis. Learning discriminative appearance-based models using partial least squares. In *SIBGRAPI*, pages 322–329, 2009. 3
- [31] J. Shawe-Taylor and N. Cristianini. *Kernel Methods for Pattern Analysis*. Cambridge University Press, 2004. 5
- [32] S. Shirazi, A. Alavi, M. T. Harandi, and B. C. Lovell. Graph-embedding discriminant analysis on riemannian manifolds for visual recognition. In *Graph Embedding for Pattern Analysis*, pages 157–175. Springer, 2013. 2, 4, 5, 6, 7, 8
- [33] R. Sivalingam, D. Boley, V. Morellas, and N. Papanikolopoulos. Tensor sparse coding for region covariances. *European Conference on Computer Vision (ECCV)*, pages 722–735, 2010. 1, 6
- [34] S. Sra. Positive definite matrices and the symmetric Stein divergence. *Preprint: [arXiv:1110.1773]*, 2012. 2
- [35] S. Sra and A. Cherian. Generalized dictionary learning for symmetric positive definite matrices with application to nearest neighbor retrieval. In *Machine Learning and Knowledge Discovery in Databases*, pages 318–332. Springer, 2011. 2, 5
- [36] P. Turaga, A. Veeraraghavan, A. Srivastava, and R. Chellappa. Statistical analysis on manifolds and its applications to video analysis. *Video Search and Mining*, pages 115–144, 2010. 2
- [37] A. Veeraraghavan, A. Roy-Chowdhury, and R. Chellappa. Matching shape sequences in video with applications in human movement analysis. *Pattern Analysis and Machine Intelligence*, 27(12):1896–1909, 2005. 1
- [38] R. Wang, H. Guo, L. S. Davis, and Q. Dai. Covariance discriminative learning: A natural and efficient approach to image set classification. In *Computer Vision and Pattern Recognition (CVPR), 2012 IEEE Conference on*, pages 2496–2503. IEEE, 2012. 6, 8